ACS Photonics

Letter

pubs.acs.org/journal/apchd5

High-Efficiency Vertical Light Emission through a Compact Silicon Nanoantenna Array

Haiyang Huang,[†,§] Hao Li,[†,§] Wei Li,[*,†,§] Aimin Wu,[*,†] Xin Chen,[†] Xuefeng Zhu,[‡] Zhen Sheng,[†] Shichang Zou,[†] Xi Wang,[†] and Fuwan Gan[*,†]

[†]State Key Laboratory of Functional Materials for Informatics, Shanghai Institute of Microsystem and Information Technology, CAS, Shanghai 200050, China

[‡]Department of Physics, Huazhong University of Science and Technology, Wuhan 430074, China

Supporting Information

ABSTRACT: Optical antennas are utilized to link free-space optical radiation with localized energy, enabling varied applications such as beam focusing, freewheeling steering, biosensing, and optical communications. Here, we demonstrate a novel silicon nanoantenna array (SNA), comprising subwavelength silicon nanorods that direct light emission vertically. When the array of nanorods was positioned optimally, the efficiency of the upward light emission reached 46%. In addition, the rigorous design of the array of nanorods resulted in a well-confined profile of the vertically emitting beam. The SNA, therefore, provides a new approach for 3D optical interconnections between different decks of integrated photonics circuits.

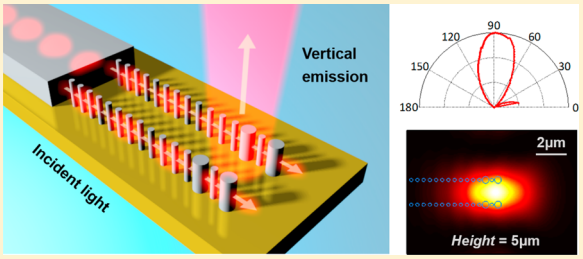

KEYWORDS: *silicon nanoantenna array, vertical light emission, 3D optical interconnection, nanophotonics*

Antennas, which link emitters and free-space propagation of electromagnetic waves, support applications in many fields, such as wireless communications, broadcasting, radar, and sensing.[1] Optical antennas have the unique capability of controlling and manipulating optical fields in optical wavelength scale; they thus hold promise for integrating photonic and electronic systems. This field has long been pursued, and various antennas have been developed. These include the Yagi-Uda antenna[2] and the bow-tie, patch, gap, and plasmonic resonator antennas.[3,4] However, up until now, the above-mentioned antennas have been of considerable size. Therefore, it is of great importance to develop more compact but still highly efficient optical antennas for silicon photonics applications.

In this Letter, we demonstrate an ultracompact silicon nanoantenna array (SNA), which is able to control light at the subwavelength scale. This is, to the best of our knowledge, the smallest silicon optical antenna built to date. This device consists of a waveguide, which is set before two parallel rows of silicon rods, which make up the nanoantennas. Each row of rods is formed by substituting two interval atoms with a pair of defect rods in the end. An in-plane optical wave is guided into the waveguide, where it is split equally between the two nanoantennas, and this generates out-of-plane far-field optical radiation on top of the defect rods. The fact that two parallel rows of rods are used forming a nanoantenna array, as shown in Figure 1a, helps to improve the vertical emission efficiency and the radiation profile of the device. The vertical beam of light generated is just a few micrometers in diameter and has a clearly defined and well-confined shape, thus providing a high potential for 3D optical interconnection. Numerical simulation shows that the theoretical upward emission efficiency of the SNA can be as high as 46%.

When designing micronano-optical devices, it is a trend to use 3D interconnection to integrate planar photonics chips with driver integrated circuit (IC) chips, and one of the intermediate layers should be composed of passive optical components.[2,5,6] This thus combines in-plane propagation with out-of-plane radiation, which serves as optical routing.[7−9] Due to its compact size and highly efficient vertical emission, as well as the combination of in-plane waveguide and out-of-plane emission, the SNA is a perfect component for such micronano-optical devices. In addition, the emission efficiency could be improved to be comparable with mature gratings through further optimization. In addition, the SNA has negligible absorption loss in contrast to its metallic counterparts at optical wavelength. Furthermore, the complementary metal-oxide semiconductor (CMOS) compatibility of the SNA makes it easily integrated with other planar optical components, even an IC, in one chip.

An SNA was derived from a single row of large-angle self-collimated silicon nanorods in which incident light can be highly localized and propagate without divergence.[10−17] Because of the excellent light-guiding function of these rods, we introduced emission properties into our SNA by inserting a single defect nanorod. A simulation model, where we used the

Received: November 9, 2015
Published: February 18, 2016

DOI: 10.1021/acsphotonics.5b00641
ACS Photonics 2016, 3, 324−328

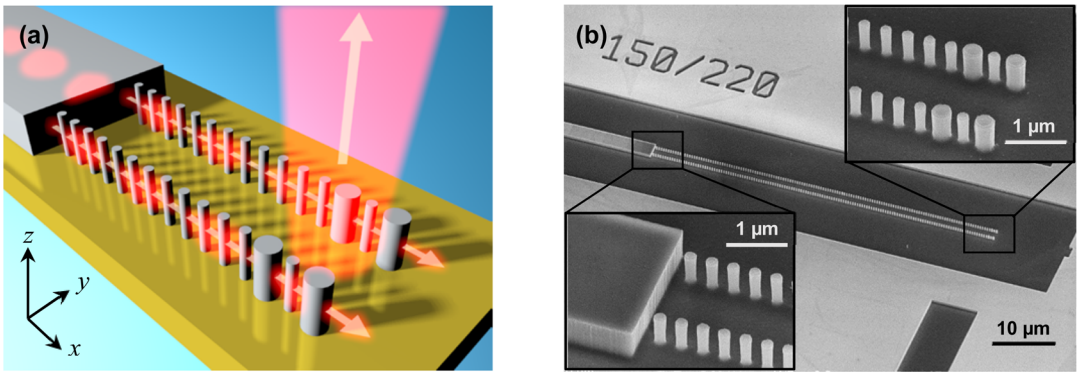

Figure 1. (a) Schematic illustration of a two-row SNA. Each SNA consists of a line of rods with a pair of defect rods at the end. Incident light at 1550 nm propagates in-plane through the waveguide (multimode) and the normal rods and is emitted vertically out-of-plane in the defect area (only the upward emission is shown). Emission light is constrained within a micrometer-scale spot. The period in the x direction (i.e., P_x) is 400 nm and in the y direction (i.e., P_y) is 1600 nm. All the rods have a height of 810 nm, and the normal rods have a radius of 110 nm, whereas the defect rods have a radius of 180 nm. The waveguide is 2.6 μm wide and 810 nm high. (b) SEM image of the fabricated structure. The inset image on the lower left shows the waveguide (on the left) and the first few rods of the SNA. The inset image in the upper right shows the defect rods. The image is taken after inductively coupled plasma deep reactive ion etching.

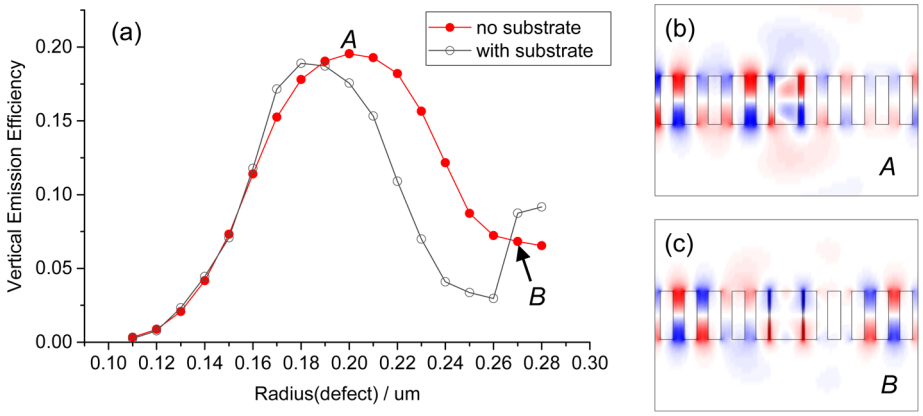

Figure 2. (a) Simulated VLE efficiency (upward emission only) in a single-defect nanorod line. The red and gray plots demonstrate that the substrate makes the peak shift. Concerning the rod line without a substrate, the radius of the defect is 0.2 and 0.27 μm in situations A and B, respectively. (b, c) Normalized E_x field distribution in the XoZ plane (y = 0) in situations A and B. The white rectangles are sectional illustrations of the structure. In this simulation, the defect rods were placed in the middle of the array.

finite-difference time-domain (FDTD) method, was employed to calculate the out-of-plane field distribution. The structure of the simulation model was composed of a row of silicon rods with a refractive index (n) of 3.45 and a separation distance (a) of 400 nm. The radius and height of the rods were 110 and 810 nm, respectively. Transverse magnetic (TM)-polarized incident light of wavelength 1550 nm could propagate through the rods with good confinement. A defect rod with varied radius was then used to replace one of the original rods. By changing the radius of the defect rod (r_{defect}) from 110 nm to 280 nm, we obtained the corresponding vertical light emission (VLE) efficiency from a field intensity monitor (dimensions 12 μm × 12 μm, in the XY plane) located 2 μm right above the defect region, as shown in Figure 2a. The VLE efficiency is defined using the following equation: VLE = E_1/E_2, where E_1 is the power of vertical light emission per unit time in the z direction and E_2 is the power of the incident light coupled to the defect rods area per unit time. The best VLE efficiency (i.e., ~19.5%) occurred when r_{defect} = 200 nm; however with defect rods of this radius, strong emission covered a comparatively wide radius range of 40 nm. The calculated E_x field distributions on the XoZ plane (y = 0) provide an explanation for this phenomenon. In the guiding mode rods area, the E_x field is mainly located in the air outside the rods. At the defect rods area, however, the change in the effective index disturbs this field. In situation A (Figure 2a), phase mismatch results in part of the E_x field penetrating into the defect rod. Some of the in-rod field is no longer confined within the rod line, and the trend is for it to leak outside in the z direction, forming the emission. In situation B, however, the index distribution is just appropriate for the E_x field to travel in and out of the defect rod with a phase reversal (Figure 2a). A major part of the E_x field passes through the defect and continues propagating. This is a descriptive analysis for VLE efficiency. In another simulation, the SiO_2 substrate was taken into consideration. The substrate breaks the symmetry in the z direction and changes the effective index of the whole structure. Accordingly, the radius of the defect rod was revised to 180 nm to achieve the highest VLE efficiency (i.e., ~18.9%).

It should be mentioned that the mechanism here is different with a leaky mode in a traditional photonic crystal.[18] For a leaky mode in a traditional photonic crystal, the changes of crystal bases lead to a change in the band structure, and the dispersion of the corresponding Bloch wave is pushed above the light cone, thus leaking into free space. While in our case, there is only a single defect, it does not impact on the band (i.e., it does

DOI: 10.1021/acsphotonics.5b00641
ACS Photonics 2016, 3, 324−328

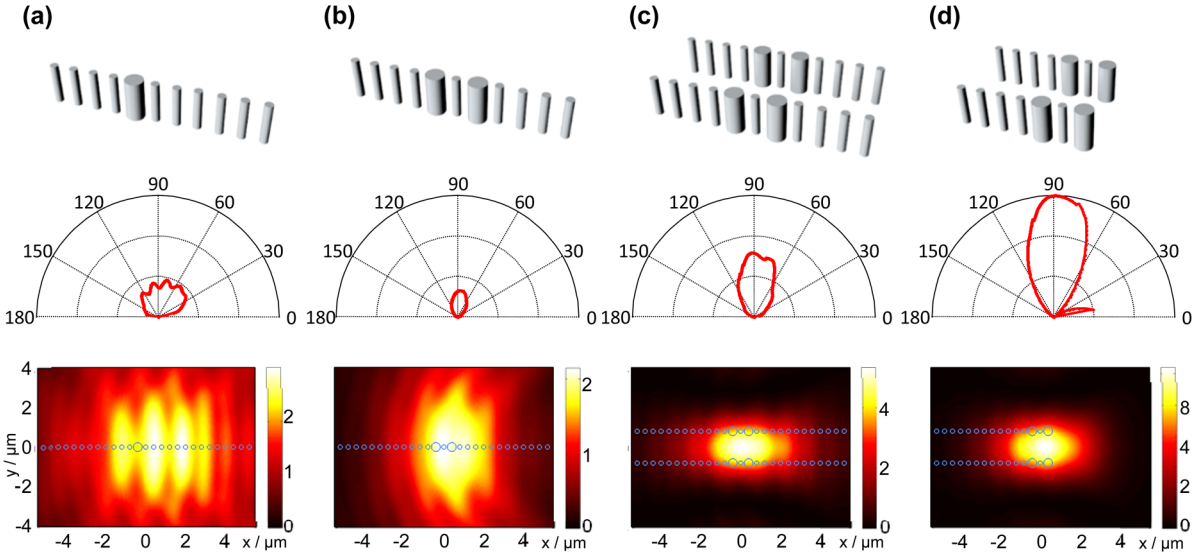

Figure 3. Testing various SNA arrays and demonstrating their antenna patterns and field profiles 5 μm above the rods. The antenna patterns were normalized to a unified scale. (a, b) Single row of nanorods containing (a) one or (b) two defect rods. (c, d) Two rows of nanorods with (c) two defect nanorods in each row and (d) as for (c) but with the end rods eliminated. The changes in structure optimize the compaction and intensity of the emission light.

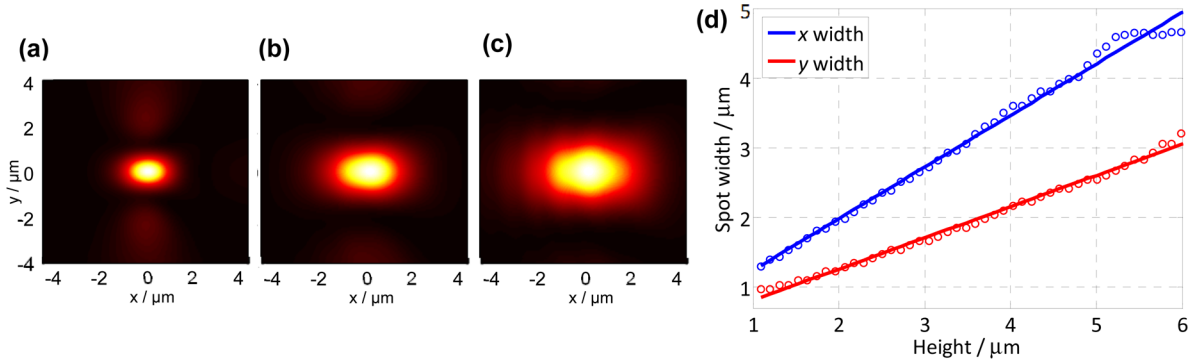

Figure 4. Emission conditions for the revised SNA. (a–c) Field profile at a height (h) of 2, 3.5, or 5 μm, respectively, which indicates good emission verticality. (d) Spot width in the x and y directions in relation to the height, which confirms a good linear increase.

not change the dispersion relation in the band frequency range).[19] The high efficiency is due to the scattering cross section of the defect. Only a proper size of the defect can achieve large emission efficiency, as shown in Figure 2a.

Moreover, further optimization was done to achieve stronger and more compact radiation. The directivity pattern of the emitted light by a single-defect structure is plotted in Figure 3a. Here, the directivity of light emission was quantified by the expression $D(\theta, \phi) = \frac{4\pi P(\theta,\phi)}{\int P(\theta,\phi)\, d\Omega}$, which is the power $P(\theta, \phi)$ per unit solid angle emitted in a particular direction divided by the emitted power per solid angle by an anisotropic source of equal total radiated power. Here, the functionality of out-of-plane emission is realized; however, more work is needed to optimize the verticality of the radiation direction. To improve the directivity of light emission in the far field, an additional defect nanorod was introduced into the line of rods. The directivity was enhanced as shown in Figure 3b, and the spot width was compressed to ~3 μm in the x direction at a height of 5 μm. Similarly, compression in the y direction could be done by adding more rows of nanorods. Considering the physical dimensions and simplicity of coupling between different rows, a double-row design was chosen to build the device. When two parallel identical nanoantennas were used to construct the SNA, the confinement of the radiation in both the x and y directions was further improved. The distance between the two rows was under rigorous design, as it directly affected the light emission. Clearly, a larger distance would lead to two individual emission profiles, while a smaller one would cause strong coupling that disturbs the emission. In order to achieve both high VLE efficiency and a compact field profile, we simulated a wide range of row distances and found 1600 nm to perform well (especially within the emission distance of 5 μm). However, more than 63% of the energy propagated through the defect area; thus the in-plane transmission was largely maintained in the rows of nanorods. In order to achieve a higher emission ratio, we eliminated all the end rods (i.e., the rods after the defect rods) and thus enhanced the reflection ratio at the end of the SNA. The reflected light propagated back through the vertical emission region once again and excited another upward emission. Both vertical emissions were constructed in free space. As a result, the directivity was further improved and the vertical emission efficiency was increased to 46%. Figure 4a–c shows the field distribution at different heights above the rods. We can see that the profile increased in a linear manner and maintained a constant shape

DOI: 10.1021/acsphotonics.5b00641
ACS Photonics 2016, 3, 324–328

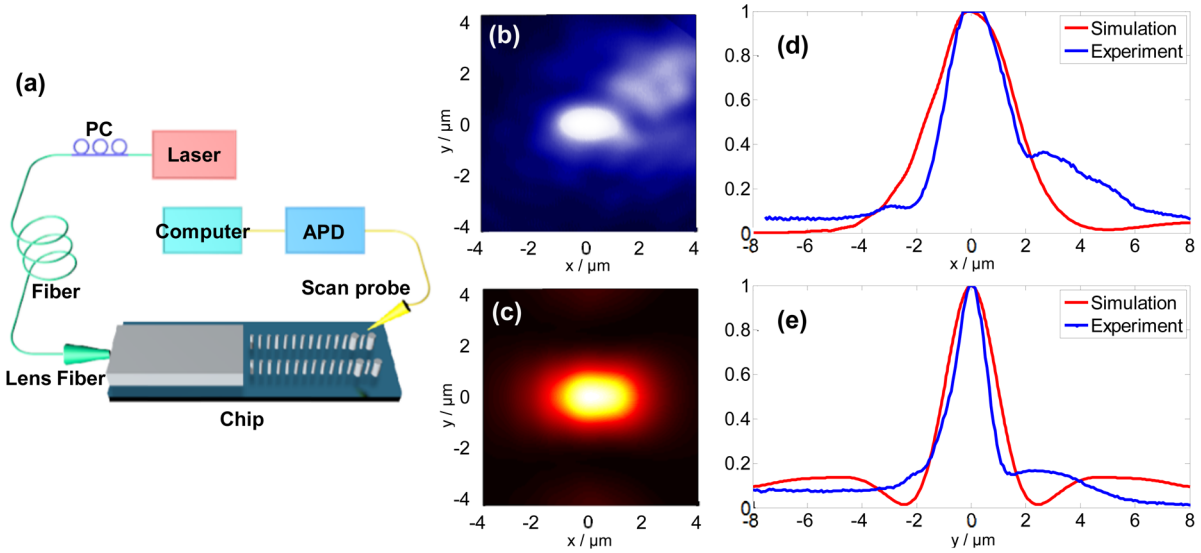

Figure 5. (a) Experimental setup for light detection. The overhead camera is not shown. PC and APD are polarization controller and avalanche photon detector, respectively. (b, c) Detected (b) and simulated (c) intensity profiles at 5 μm above the defect area. (d, e) Normalized field intensity distribution comparison for the experimental and simulation results in the x (d) and y (e) direction.

as the height increased. Also, the central position of the profile remained stable at the different heights. These optimized properties are suitable for various practical applications in 3D optical assembling.

Finally, a slab waveguide was put in front of the SNA to couple the incident light equally into the two rows. When the mode profile at the output side of the waveguide and the two rows match, high coupling efficiency could be expected (similarly to a multimode interference coupler). This was mainly determined by the physical parameters of the waveguide when the design of the SNA is already fixed. In our design, a multimode waveguide, which was 2.6 μm wide, 7.1 μm long, and 0.81 μm high, was used to fulfill the high efficiency coupling, reaching 92.3% in simulations. In order to facilitate the test, the waveguide was extended to 700 μm in the experiment.

After simulation testing, we fabricated an SNA on a silicon-on-insulator (SOI) substrate, where the top silicon layer and buried oxide layer were 810 nm and 3 μm thick, respectively. The top silicon layer was then coated with a 60 nm thick thermal oxide layer to form a hard mask. The pattern was transferred to the hard mask via e-beam lithography followed by reactive ion etching. Finally, the SNA was sculpted by an elaborate ICP-DRIE (inductively coupled plasma deep reactive ion etch) process. The fabricated SNA, which consists of two identical parallel rows of nanorods and covers a distance of 1600 nm, is shown in Figure 1b. The SNA is composed of two rows of silicon nanorods, and the period and the radius are 400 and 110 nm, respectively. The radius of each of the defect nanorods used in this structure is 180 nm.

We measured the emission light spot of the sample with a Nanonics MultiView 4000 scanning near-field optical microscope (SNOM). As is shown in Figure 5a, a TM-polarized (i.e., E_z-polarized) light beam was first coupled from a lensed fiber to a waveguide, which was integrated with the SNA on the same substrate. The silicon waveguide then directed the beam toward the array. An overhead camera was used to assist with the alignment of the fiber and the waveguide. A scanning aperture probe (the aperture size is 200 nm), which could be automatically controlled to scan in the XY plane, was first set to touch the sample. Then the probe rose 5 μm (in the z-direction) and scanned above the SNA in the XY plane to record the field distribution from the array. It should be mentioned that the actual field detected was the far field, and it is still within the ability of the SNOM. The wavelength used in the measurements was 1550 nm.

The field intensity profile, detected 5 μm above the defect area of the SNA, is shown in Figure 5b. The corresponding simulated profile and comparison charts of the normalized distribution in the x and y direction are also given in Figure 5c–e. The shape of the profile is a subellipse, which is even more compact than that demonstrated in the simulation. Based on the fwhm (full width at half-maximum), we calculated that the spot size in the experiment was ~2.8 μm × 1.6 μm. The compact size of the spot also indicates that the design provides excellent tolerance against some random small process errors that might have occurred during fabrication. Apart from the small tilt in the tail of the spot, the experimental results were consistent, in both distribution and size, with those obtained during the simulation.

In conclusion, we have demonstrated both by numerical simulation and then by fabrication and experimentation that a novel SNA can direct light emission into the third dimension. In the simulation, the SNA exhibited a maximal light vertical emission efficiency of 46%, which indicates that it can provide superior directional properties. In addition, the structure can generate a far-field micrometer-scale radiation pattern, which expands in a slow and linear manner. We suggest that being just one wavelength in size, this is the smallest SNA developed to date, and we propose that this optical emitter will be a key component for the future development of 3D optical interchip interconnections with multilayered nanophotonic chips based on CMOS technology.

■ ASSOCIATED CONTENT

Supporting Information

The Supporting Information is available free of charge on the ACS Publications website at DOI: 10.1021/acsphotonics.5b00641.

DOI: 10.1021/acsphotonics.5b00641
ACS Photonics 2016, 3, 324−328

Differences between the emission of the SNA and the photonic crystals' leaky modes; field profiles at higher positions (PDF)

AUTHOR INFORMATION

Corresponding Authors

*E-mail: waylee@mail.sim.ac.cn (W. Li).
*E-mail: wuaimin@mail.sim.ac.cn (A. Wu).
*E-mail: fuwan@mail.sim.ac.cn (F. Gan).

Author Contributions

§H. Huang, H. Li, and W. Li contributed equally.

Notes

The authors declare no competing financial interest.

ACKNOWLEDGMENTS

This work was supported by National Natural Science Foundation of China (Grants 61275112, 61401443, 61475180, and 11204340), Science and Technology Commission of Shanghai Municipality (Grant 14JC1407600), and the National Natural Science Foundation of China (Grant 11404125). The scanning near-field optical microscopy and related experiments were supported by the State Key Laboratory of Advanced Optical Communications and Networks, Peking University, Beijing, China.

REFERENCES

(1) Maß, T. W.; Taubner, T. Incident angle-tuning of infrared antenna array resonances for molecular sensing. *ACS Photonics* **2015**, *2*, 1498−1504.

(2) Dregely, D.; Taubert, R.; Dorfmüller, J.; Vogelgesang, R.; Kern, K.; Giessen, H. 3D optical Yagi-Uda nanoantenna array. *Nat. Commun.* **2011**, *2*, 267.

(3) Li, Z.; Butun, S.; Aydin, K. Touching gold nanoparticle chain based plasmonic antenna arrays and optical metamaterials. *ACS Photonics* **2014**, *1*, 228−234.

(4) Ren, M.; Chen, M.; Wu, W.; Zhang, L.; Liu, J.; Pi, B.; Zhang, X.; Li, Q.; Fan, S.; Xu, J. Linearly polarized light emission from quantum dots with plasmonic nanoantenna arrays. *Nano Lett.* **2015**, *15*, 2951−2957.

(5) Roelkens, G.; Liu, L.; Liang, D.; Jones, R.; Fang, A.; Koch, B.; Bowers, J. III-V/silicon photonics for on-chip and intra-chip optical interconnects. *Laser Photonics Rev.* **2010**, *4*, 751−779.

(6) Sun, J.; Timurdogan, E.; Yaacobi, A.; Hosseini, E. S.; Watts, M. R. Large-scale nanophotonic phased array. *Nature* **2013**, *493*, 195−199.

(7) Wu, A.; Li, H.; Du, J.; Ni, X.; Ye, Z.; Wang, Y.; Sheng, Z.; Zou, S.; Gan, F.; Zhang, X. Experimental demonstration of in-plane negative-angle refraction with an array of silicon nanoposts. *Nano Lett.* **2015**, *15*, 2055−2060.

(8) Du, J.; Liu, S.; Lin, Z.; Zi, J.; Chui, S. Guiding electromagnetic energy below the diffraction limit with dielectric particle arrays. *Phys. Rev. A: At., Mol., Opt. Phys.* **2009**, *79*, 051801.

(9) Du, J.; Lin, Z.; Chui, S.; Lu, W.; Li, H.; Wu, A.; Sheng, Z.; Zi, J.; Wang, X.; Zou, S. Optical beam steering based on the symmetry of resonant modes of nanoparticles. *Phys. Rev. Lett.* **2011**, *106*, 203903.

(10) Gan, L.; Qin, F.; Li, Z.-Y. Broadband large-angle self-collimation in two-dimensional silicon photonic crystal. *Opt. Lett.* **2012**, *37*, 2412−2414.

(11) Lin, S.-Y.; Chow, E.; Hietala, V.; Villeneuve, P. R.; Joannopoulos, J. Experimental demonstration of guiding and bending of electromagnetic waves in a photonic crystal. *Science* **1998**, *282*, 274−276.

(12) Lu, Z.; Shi, S.; Murakowski, J. A.; Schneider, G. J.; Schuetz, C. A.; Prather, D. W. Experimental demonstration of self-collimation inside a three-dimensional photonic crystal. *Phys. Rev. Lett.* **2006**, *96*, 173902.

(13) Arlandis, J.; Centeno, E.; Pollès, R.; Moreau, A.; Campos, J.; Gauthier-Lafaye, O.; Monmayrant, A. Mesoscopic self-collimation and slow light in all-positive index layered photonic crystals. *Phys. Rev. Lett.* **2012**, *108*, 037401.

(14) Li, H.; Wu, A.; Li, W.; Lin, X.; Qiu, C.; Sheng, Z.; Wang, X.; Zou, S.; Gan, F. Millimeter-scale and large-angle self-collimation in a photonic crystal composed of silicon nanorods. *IEEE Photonics J.* **2013**, *5*, 2201306−2201306.

(15) Joannopoulos, J. D.; Johnson, S. G.; Winn, J. N.; Meade, R. D. *Photonic Crystals: Molding the Flow of Light*; Princeton University Press, 2011.

(16) Prather, D. W.; Shi, S.; Murakowski, J.; Schneider, G. J.; Sharkawy, A.; Chen, C.; Miao, B.; Martin, R. Self-collimation in photonic crystal structures: a new paradigm for applications and device development. *J. Phys. D: Appl. Phys.* **2007**, *40*, 2635.

(17) Mocella, V.; Cabrini, S.; Chang, A.; Dardano, P.; Moretti, L.; Rendina, I.; Olynick, D.; Harteneck, B.; Dhuey, S. Self-collimation of light over millimeter-scale distance in a quasi-zero-average-index metamaterial. *Phys. Rev. Lett.* **2009**, *102*, 133902.

(18) Zhang, H.; Zhu, H.; Qian, L.; Fan, D. Analysis of leaky modes of photonic crystal slabs with deeply patterned lattice. *J. Opt. A: Pure Appl. Opt.* **2006**, *8*, 483.

(19) Cheng, L.; Wei, L.; Xun-Ya, J.; Jun-Cheng, C. Effect of disorder on hyperbolic metamaterials. *Chin. Phys. B* **2014**, *23*, 097802.

DOI: 10.1021/acsphotonics.5b00641
ACS Photonics 2016, 3, 324−328